Final Draft

of the original manuscript

André, N.; dos Santos, J.; Amancio-Filho, S.:

Impact resistance of metal-composite hybrid joints produced by frictional heat.

In: Composite Structures. Vol. 233 (2020) 111754.

First published online by Elsevier: 30.11.2019

https://dx.doi.org/10.1016/j.compstruct.2019.111754

"Impact resistance of metal-composite hybrid joints produced by frictional heat"

Natalia M. André[1], Jorge F. dos Santos[1], Sergio T. Amancio-Filho[2*]

[1] Helmholtz-Zentrum Geesthacht, Centre for Materials and Coastal Research, Institute of Materials Research, Materials Mechanics, Solid State Joining Processes, Geesthacht, Germany

[2] Graz University of Technology – TU Graz, Institute of Materials Science, Joining and Forming, BMVIT Endowed Professorship for Aviation, Kopernikusgasse 24/1, 8010 Graz – Austria

*Corresponding author: Tel./Fax: +43 (0) 316 873-1610/ 7187 email: sergio.amancio@tugraz.at

Abstract

The impact resistance of aluminum alloy 2024-T3 and carbon-fiber-reinforced polyphenylene sulfide joints was investigated using drop weight test. The joints were aluminum-side and composite-side impacted to provide a preliminary design guideline for hybrid joints. Four energy levels were investigated for each side: 2 J, 4 J, 6 J and 8 J. The joints presented rebounding behavior for all the energy levels. It implies that in all the cases, the impact energy was not totally absorbed by the joints, although the joints failed at 8 J of impact energy. The interface of the joint presented its threshold for absorption of impact energy around 6.5 J, which was reached when the joint was impacted with 8 J of potential energy, independently of the surface under impact. Thus, this study showed that a single friction spot joint could absorb up to 103 $kJ.m^{-2}$ of joined area. The joints impacted from the aluminum side presented residual strengths of 84% (2 J), 30% (4 J), and 25% (6 J). For composite-side impacted joints, the residual strengths were 80% (2 J), 54% (4 J), and 45% (6 J). Generally, the aluminum-side impacted joints showed lower residual strength than the composite-side impacted joints. The impact energy introduced from the aluminum side was mostly absorbed in the plastic deformation of the aluminum part, bending the aluminum and promoting the detachment of the interface. Otherwise, the impact energy introduced from the composite side was mostly absorbed by the creation/extension of internal damage through the plies of the composite. Thus, it is expected that the impact energy was only partially transferred to the interface of the joint in the case of composite-side impact. Consequently, these joints presented higher residual strength after impact than the aluminum-side impacted joints.

Keywords: Friction Spot Joining, aluminum alloys, fiber reinforced composites, drop weight impact, damage tolerance

1. Introduction

Accidental impacts on aircraft and automobile structures are often reported during manufacturing, shipping, maintenance and daily operations. In cooperation with airlines, a study by Airbus has stated that the main aircraft areas subjected to impact are the surrounding of the doors (53%), the doors (15%) and the wings (13%) [1]. The impact threat levels for each aircraft zone were investigated and the results indicated that impact energies below 35 J were the most common extent of damage [1].

Preexisting and in-service accidental damages can strongly affect the performance and hence the safety of structural components [2]. Therefore, predicting the load or time for a sub-critical damage to sufficiently accumulate to cause a premature failure is significantly important to ensure a robust and safe structure [2,3].

Promoted by the new economic and environmental policies, the combination of lightweight metal alloys and fiber-reinforced polymers have become an alternative solution for saving weight and fuel in the transport industry [4,5]. The concept of metal-composite hybrid structures is a promising solution mainly due to the optimal specific strength and stiffness associated to these materials [4,5]. A recent example of hybrid structures use is the A350 XWB. This aircraft launch has set a new standard at Airbus with the use of 53 wt% composites in its structure contributing to a reduction of 25% in fuel consumption [1]. However, due to the high dissimilarity of their properties, composites and metals respond differently to in-service loading and accidental damage [2,6,7]. For instance, impact damage in metallic materials can be usually detected visually during maintenance, while in composites, the impact energy is absorbed as internal defects that cannot be detected visually [1]. The strength degradation is also very diverse. For metals, the damage usually starts with plastic deformation [8]. Thus, there is no immediate loss in performance and the deformation of the component is usually spotted easily [2]. For composites, however, the damage develops through complex mechanisms of delamination and bridging, which may lead to an immediate reduction in performance depending on the type of composite and the extent of damage [2,9]. Therefore, the assessment of the impact resistance of such hybrid structures is of great importance, not only to predict premature failure and damage tolerance, but also to guide the design of such hybrid structures [2,10].

Considering the impact behavior of fiber metal laminates (FML), Liu and Liaw [11] investigated the influence of the metal constituent in the impact behavior of GLARE. In case AA7475-T6 was used, small deflections were identified after impact due to the high stiffness of this material. Nevertheless, earlier crack initiation was observed for AA7475-T6 in comparison to a more ductile aluminum alloy, such as AA2024-

T3. The authors reported that by using AA2024-T3 instead of AA7475-T6, smaller damage zones were created due to impact. In the case of AA2024-T3, more energy was attenuated through plastic deformation than for AA7075-T6.

Silva *et al.* [12] assessed the impact behavior of adhesively bonded high strength steel joints. The authors produced the joints using a flexible adhesive at the ends of the overlap, while a rigid adhesive was applied in the middle of the joint. This mixed-adhesive strategy improved the impact resistance of the joints, as a result of mixed ductile-brittle failure mechanisms. They showed that in this case, 100 % of the impact energy was absorbed, in contrast with only 50 % of absorption when only one type of adhesive was employed. In another study, Machado *et al.* [13] performed a similar study for CFRP bonded joints. The effects of combining flexible and rigid adhesives were found to be similar as what was observed for steel joints. Nevertheless, higher impact failure loads were observed for the CFRP joints in comparison to the steel joints. It is believed that the internal damages created in the CFRP substrates reduced the stresses in the adhesive layer of these joints in comparison to the steel joints, thus preserving their strength.

Friction Spot Joining (FSpJ) is an alternative joining technology for metal-polymer/composite structures. Patented in 2011 [14], this technology uses a non-consumable tool to create frictional heat and plastically deform the metallic component of the overlap joint [15]. The main bonding mechanisms of friction spot joints are mechanical interlocking and adhesion forces [16]. The mechanical interlocking is created in macro- and micro-scales through the deformation of the metal into the composite part ("metallic nub") and the attachment of fibers and matrix to the metal surface, respectively [16]. Additionally, a layer of polymer close to the joint interface is melted during the joining process. After the cooling of the joint, the layer of molten polymer reconsolidates, establishing the adhesion forces between metal and polymer/composite [16].

Goushegir *et al.* [17] successfully demonstrated the feasibility of FSpJ for aluminum alloy 2024-T3 and carbon-fiber-reinforced polyphenylene sulfide (CF-PPS) joints. Shear strengths from 38 up to 123 MPa were achieved using different surface pre-treatments. Other combinations of materials have also been investigated. Among studies published recently, André *et al.* [18] used AA2024-T3/PPS/CF-PPS, Esteves *et al.* [19] used AA6181-T4/CF-PPS and Amancio *et al.* [15] studied AZ31-O/GF- and CF-PPS. Despite the high levels of quasi-static mechanical performance reported for friction spot joints in previous investigations, the impact resistance of the joints has not been addressed yet.

The present study investigated the impact resistance of AA2024/CF-PPS friction spot joints using the drop weight test. Four levels of impact energy were tested: 2 J, 4 J, 6 J and 8 J. The joints were aluminum-side and composite-side impacted to provide a preliminary design guideline regarding the impact damage tolerance of such hybrid joints. The absorbed energy and the development of damage on the aluminum and composite surfaces were analyzed for the different impact energies under study. Laser scanning microscopy was used to monitor the damage evolution on the surfaces. Ultrasonic echo scanning was applied to evaluate internal damage in the interface and in the composite part of the joints. Finally, the transfer of the impact energy to the interface of the joint was assessed and correlated to the residual strength of the joints, according to the side of the joint under impact.

2. Materials and Methods

2.1. Aluminum alloy 2024-T3

Aluminum alloy 2024-T3 2 mm thick rolled sheets were used as the metal part in this study. It is a precipitation hardenable alloy supplied by Costellium (France). The main alloying elements are Cu and Mg. This alloy is widely used in the aircraft industry due to its good specific strength and fatigue performance [20]. Table 1 presents the chemical composition of the alloy used in this work. Table 2 lists the selected physical and mechanical properties of this alloy [21].

Table 1: Nominal chemical composition of AA2024-T3

Element	Cu	Mg	Mn	Fe	Zn	Si	Ti	Cr	Al
Wt%	4.55	1.49	0.45	0.17	0.16	0.10	0.02	<0.01	Bal.

Table 2: Selected physical and mechanical properties of AA2024-T3 [21].

Tensile Strength (TL direction) [MPa]	Yield Strength (TL direction) [MPa]	Elongation [%]	Incipient Melting Temperature [°C]	Thermal Conductivity [W m^{-1} K^{-1}]	Coefficient of Thermal Expansion , 20–300°C [µm m^{-1} $°C^{-1}$]
437	299	21	502	121	24.7

2.2. Carbon-fiber-reinforced polyphenylene sulfide (CF-PPS)

This work used carbon-fiber-reinforced polyphenylene sulfide (CF-PPS) as the composite part. This is a quasi-isotropic laminate that is 2.17 mm thick with 43 wt% carbon fibers woven fabric (5H satin

111 configuration). The composite consists of seven plies of carbon fiber fabric reinforcement in the
112 $[(0.90)/(\pm 45)]_3/(0.90)$ sequence. CF-PPS is a high-performance thermoplastic composite and has several
113 aerospace applications [22]. The "J-Nose" subframe wings of Airbus A380 and the pylon covers of Airbus
114 A320 are examples of the application of such material [22,23]. Table 3 presents a selection of relevant
115 physical and mechanical properties of the CF-PPS.

116 Table 3: Selected physical and mechanical properties of the CF-PPS [22].

Tensile Strength (warp/weft) [MPa]	In-Plane Shear Strength [MPa]	Glass Transition Temperature [°C]	Melting Temperature [°C]	Thermal Conductivity [W m^{-1} K^{-1}]	Coefficient of Thermal Expansion, 23–300°C [µm m^{-1} $°C^{-1}$]
790/750	119	120	280	0.19	52.2

117

118 **2.3. Experimental Procedure**

119 **2.3.1. Joining procedure**

120 The aluminum part was sandblasted before the joining process to increase its surface roughness.
121 Previous investigations [17,24] have shown that such mechanical surface pre-treatment enhances the
122 adhesion between aluminum and composite. The medium blast used was corundum (Al_2O_3, average particle
123 size: 100–150 µm). The aluminum parts were sandblasted for 10 s at a distance of 20 cm, and an incidence
124 angle of 45° of the blasting pistol. An average surface roughness (R_a) of 6.7 ± 0.4 µm was obtained.

125 The joints were produced in a single overlap configuration, as depicted in Figure 1. The FSp
126 joining equipment RPS 200 (Harms & Wende, Germany) was used.

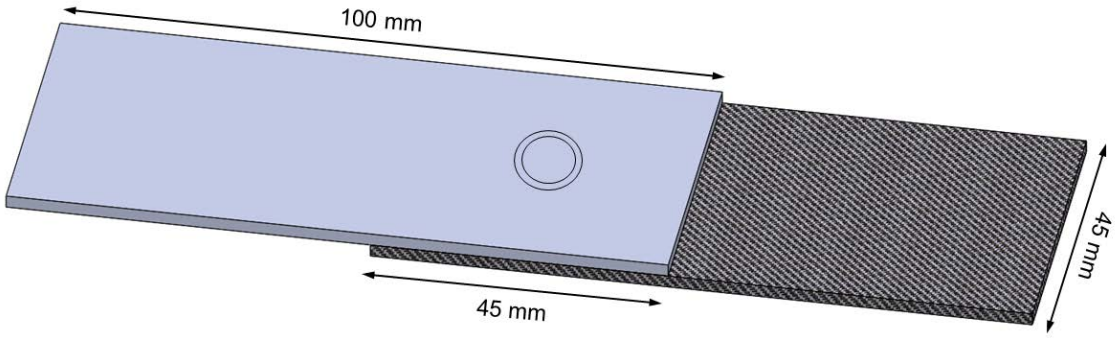

127

128 Figure 1: Configuration and dimensions of the joints (in mm).

129 The parts were joined using 2900 rpm of rotational speed, 0.8 mm of plunge depth, 8 s of joining
130 time and 6 kN of joining force. This combination of joining parameters maximized the lap shear strength
131 of the joints and it was obtained from a previous statistical optimization (design of experiments combined

with analysis of variance). A three-piece tool consisting of pin, sleeve and clamping ring was used (Figure 2). The sleeve-plunge variant of FSpJ was employed to produce the joints in this study. Figure 2 describes the main steps of the FSpJ process: (1) positioning of the parts under the tool, plunging of the sleeve into the metal, plasticization and deformation of the metal part, (2) refilling of the keyhole formed by the sleeve plunging, and (3) consolidation of the joint under pressure. For details about the FSpJ process, please refer to [17].

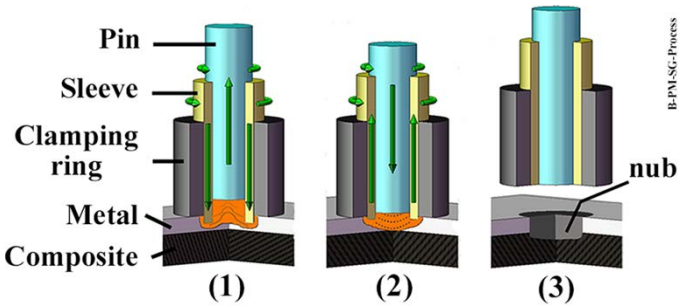

Figure 2: Steps of the FSpJ process: (1) plunging of the sleeve and plasticization of the metal, (2) refilling of the keyhole, and (3) joint consolidation (Adapted from [17]).

2.3.2. Drop weight test

An instrumented drop weight tower was used to perform the drop weight tests. The tower was equipped with an anti-rebound system to avoid secondary impacts. The overlap area of the joints was clamped between cylindrical pneumatic clamping fixtures, as shown in Figure 3. A semi-spherical impactor with a radius (r) of 6.25 mm was used. The specimens were impacted in the center of the overlap area where the spot joint was produced. Four levels of impact energy were investigated: 2 J, 4 J, 6 J and 8 J. These levels of impact energy were chosen after a first assessment of the impact resistance of the friction spot joints. In this way, damages starting from barely visible up to the complete failure of the joint were covered. In order to provide a preliminary design guideline on the impact damage tolerance of such hybrid joints, the specimens were impacted from both facets, i.e., one set of the specimens from the aluminum side (AS) and another set from the composite side (CS). The load applied by the impactor on the specimens was measured during the impact events by a strain gauge full bridge placed on the head of the impactor. Three replicates were tested for each energy level.

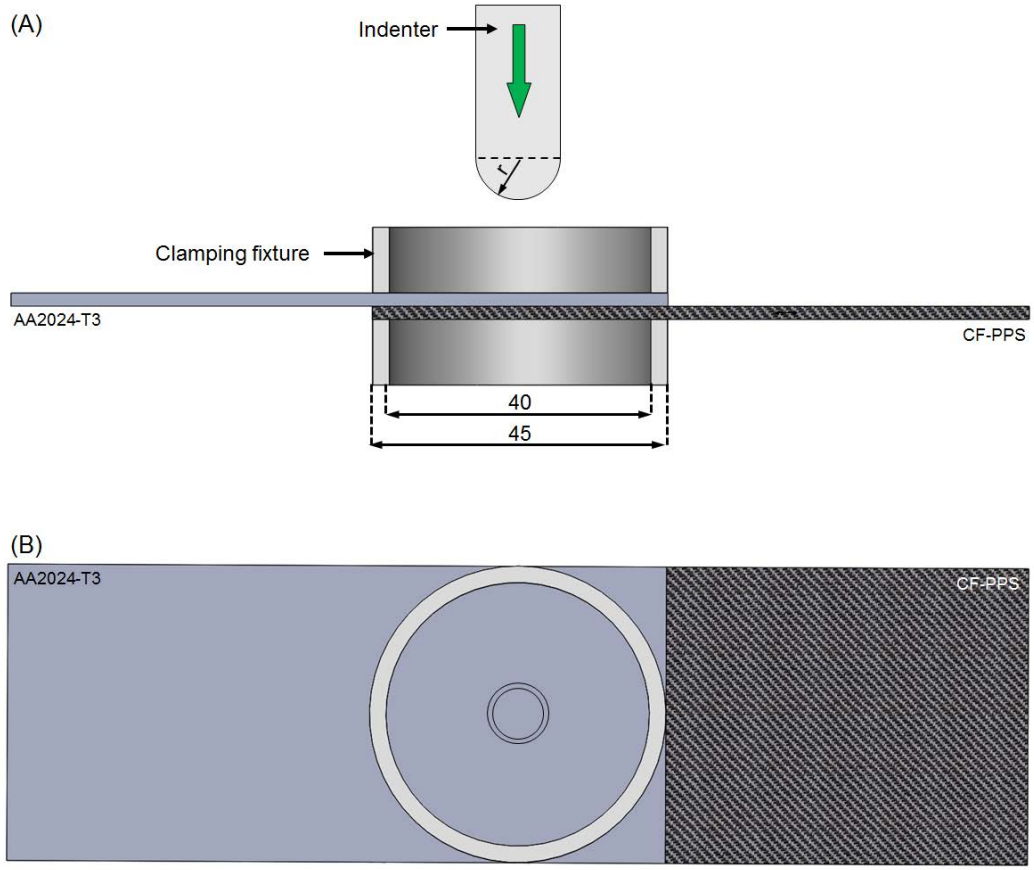

Figure 3: Schematics of the clamping of the specimens during drop weight test. (A) Side view and (B) top view of the configuration used in this work.

2.3.3. Non-destructive inspection

Confocal laser scanning microscopy (VK-9700, Keyence, Japan) was employed to generate 3D profiles of the impacted region of the joints. The damage area and depth were also measured from the 3D profiles.

Another non-destructive inspection of the joints was performed with an automated ultrasonic scanning system (USPC 3040, Dr. Hillger, Germany) based on a single pulse-echo sensor. The overlap area of the specimens was scanned from the composite side of the joint to investigate the damage evolution through the plies of the composite. Additionally, scanning from the aluminum side of the joints was also performed to evaluate the adhesion at the metal-composite interface after impact. A frequency of 1 MHz and speeds of 2700 ms^{-1} and 1600 ms^{-1} were employed to scan the composite and the aluminum parts, respectively. The measurements were performed with a resolution of 0.1 mm. Figure 4 exemplifies the ultrasonic scanning from the aluminum side of the joint.

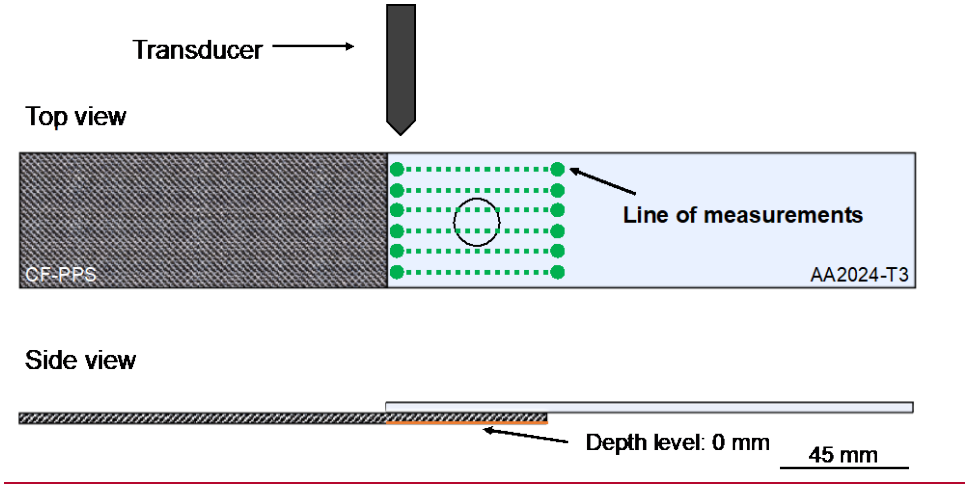

Figure 4: Schematics of the ultrasonic scanning, here depicting the scanning on the aluminum surface of the friction spot joint.

2.3.4. Shear after impact test (ShAI)

Lap shear testing under tensile loading was performed to assess the residual strength of the joints after impact. Such tests are known as shear after impact (ShAI), and are widely applied in the aircraft industry to assess the impact damage tolerance of composite structures [25]. The tests were performed using a universal testing machine Zwick/Roell 1478 Germany, 100 kN load cell, cross-head speed of 1.27 mm min^{-1} and at room temperature. Specimens with dimensions of 100 x 45 mm (2025 mm^2 of overlap area) were tested, as depicted in Figure 1. No tabs were used in this case since the grips of the test machine were offset to accommodate the overlap configuration of the specimens. The average residual shear strength of the joints was evaluated on three replicates for each impact condition.

3. Results and Discussion

3.1. Impact loading and energy absorption

Figure 5 presents representative force-time curves obtained during the impact events for the different energy levels and the configurations investigated in this work.

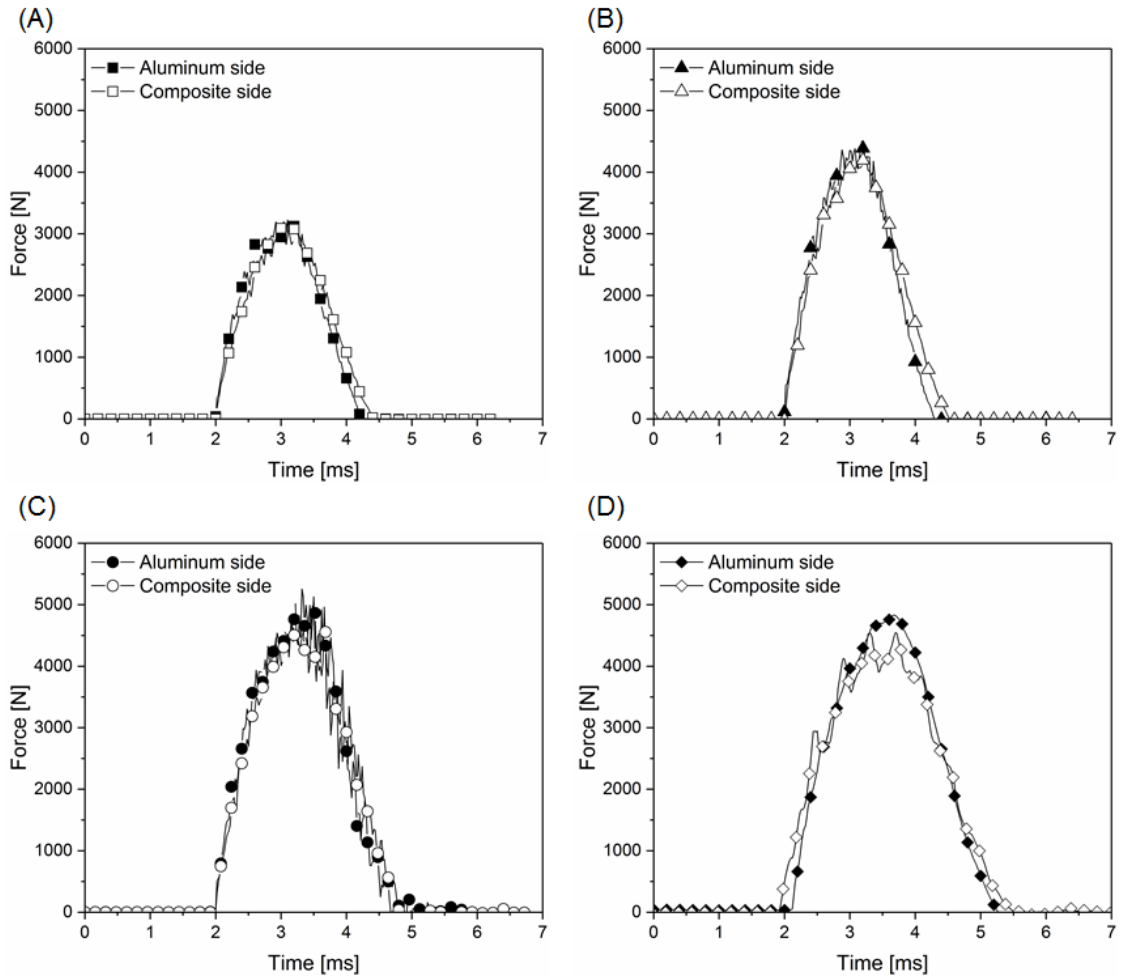

Figure 5: Representative force-time histories of aluminum-side (AS) and composite-side (CS) impacted joints for (A) 2 J, (B) 4 J, (C) 6 J and (D) 8 J of potential energy. The failure of the joints occurred at 8 J for both AS and CS cases.

The force-time curves show the loading and unloading of the joint during the impact event. The curves present a few oscillations during loading and unloading. One notes that the density of oscillations increases significantly from 2 J to 6 J and then decreases at 8 J, when the failure under impact of the joints occurred. Such oscillations can be related either to vibrations of the structure due to acceleration and deceleration of the joint during the impact event and/or the occurrence of internal damage in the joint [26,27]. The internal damage created during impact on the joint interface, as well as on the composite part, is discussed in Section 3.2.

Figure 6 shows the maximum forces achieved in each energy level for the aluminum-side and the composite-side impacted joints. The maximum force achieved during impact increases linearly from 2 J to

6 J of impact energy. At 8 J, the failure under impact of the joints occurred. At this energy level, it is observed that the maximum force achieved is statistically the same as the force achieved at 6 J (6 J: 5440 ± 186 N (AS)/5085 ± 162 N (CS); 8 J: 5305 ± 125 N (AS)/4987 ± 345 N (CS)). Thus, it suggests that the failure threshold for impact force is approximately 5204 ± 178 N for a single friction spot joint.

It is important to note that for each energy level, the load applied by the impactor in the joint is very similar, independently of the surface under impact (Figures 5 and 6). One observes that when impacted from the aluminum side, the joint is subjected to a slightly higher force (Figure 6). However, considering the standard deviation of such values, the difference between the maximum force achieved from the aluminum and the composite impacted surfaces are statistically insignificant.

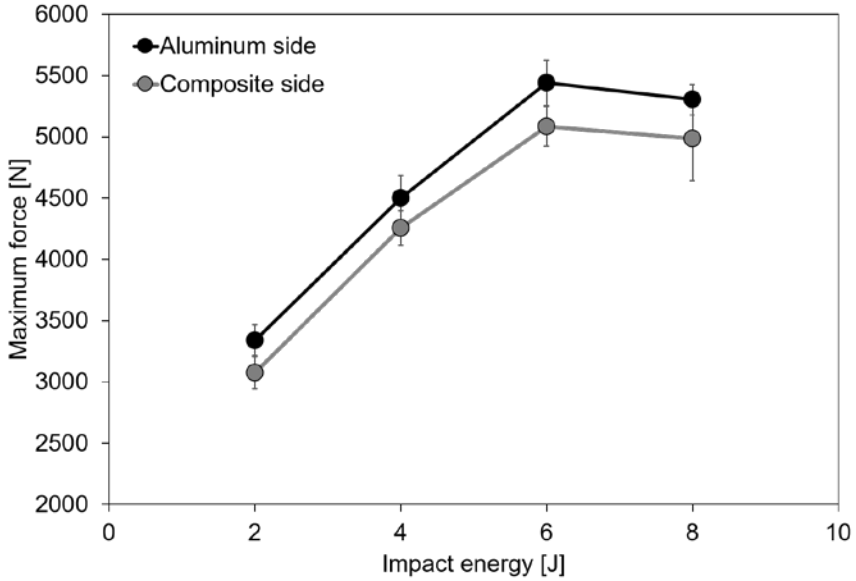

Figure 6: Maximum force applied to the joints during impact for the different energy levels. The failure of the joints occurred at 8 J of impact energy.

The absorbed energies during impact were calculated from the force-time curves in Figure 5. Based on the Energy Profile Method (EPM) [27–30], Figure 7 depicts the energy profile obtained for the single friction spot joints in this study. Figure 7 demonstrates that the joints presented rebounding behavior for all the investigated energy levels, independently of the surface under impact, i.e. all impacted joints are situated under the equal energy line in Figure 7. It implies that for all the cases under study, the impact energy was not totally absorbed by the joints. In contrast, the joint failed at 8 J of impact energy. It suggests that aluminum and composite could further absorb energy during an impact event. Nevertheless, the interface

of the joint reached its threshold at 8 J of impact energy, when 6.5 J was absorbed, independently of the surface under impact (Figure 7). Considering that a friction spot joint has a nominal joined area of about 63.6 mm^2, it indicates that a single friction spot joint could absorb up to 103 $kJ.m^{-2}$ of joined area.

Machado *et al.* [13] investigated several combinations of adhesives to maximize the impact resistance of CF-epoxy bonded joints for automotive applications. They demonstrated that the combination of a flexible adhesive (in the edges of the overlap) and a stiff adhesive (in the center of the overlap) led to optimized energy absorption during impact. In this case, energy absorption up to 48 kJ m^{-2} of bonded area was achieved, approximately half of the intake of a friction spot joint.

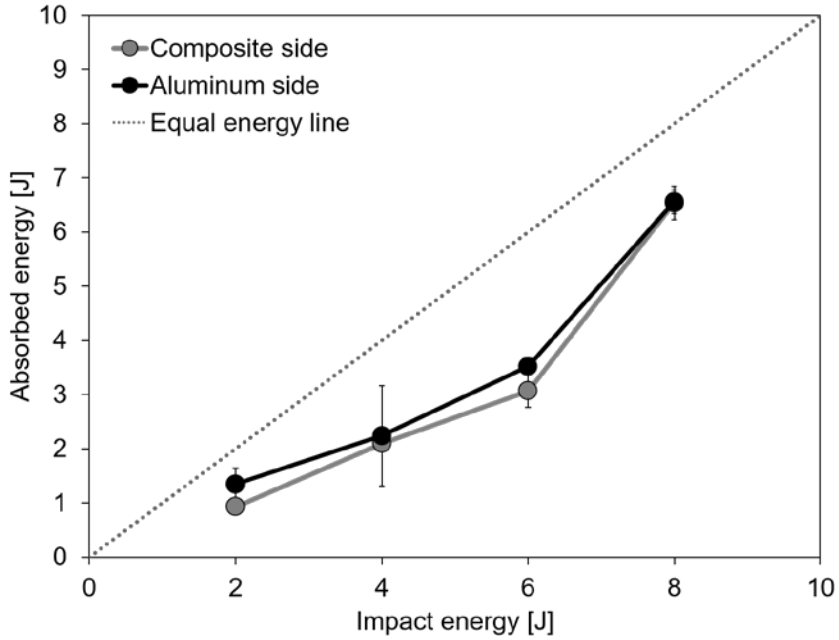

Figure 7: Energy profile obtained for single friction spot joints in this study. The failure of the joints occurred at 8 J of impact energy.

3.2. Impact damage and its transfer to the joint interface

Figure 8 presents the area and the maximum depth of impact damage identified on the aluminum and the composite surfaces for the different levels of impact energy under investigation. One observes that both the area and the depth of damage increase with the rise of impact energy, independently of the side (AS or CS) under impact. The damage area increased from 4.6 ± 0.3 mm^2 (2 J) to 12.7 ± 0.2 mm^2 (8 J) for the aluminum-side impacted joints; an increase of 64%. For the composite-side impacted joints, the increase in damage area was 44%; 10.4 ± 1.4 mm^2 (2 J) to 18.8 ± 0.7 mm^2 (8 J). Simultaneously, the damage depth increased 90% when the impact energy was raised from 2 J to 8 J for the aluminum-side impacted joints

(5.1 ± 0.3 µm (2 J) to 47.3 ± 0.2 µm (8 J)). For the composite-side impacted joints the increase in damage depth was 69% (81.2 ± 8.7 µm (2 J) to 260.3 ± 7.4 µm (8 J)).

The observations from Figure 8 demonstrate that the damage evolves differently depending on which side of the joint is subjected to impact. One can observe that at the same level of impact energy, the damage caused on the composite surface is deeper and roughly twice the size of the damage caused on the aluminum surface. Such differences in damage development were expected, considering the diverse structures and mechanical properties of the aluminum alloys and the fiber-reinforced thermoplastics [31]. The damage development and its consequence on the transfer of impact energy to the joint interface are discussed for both cases (aluminum-side and composite-side impact) in the following sections.

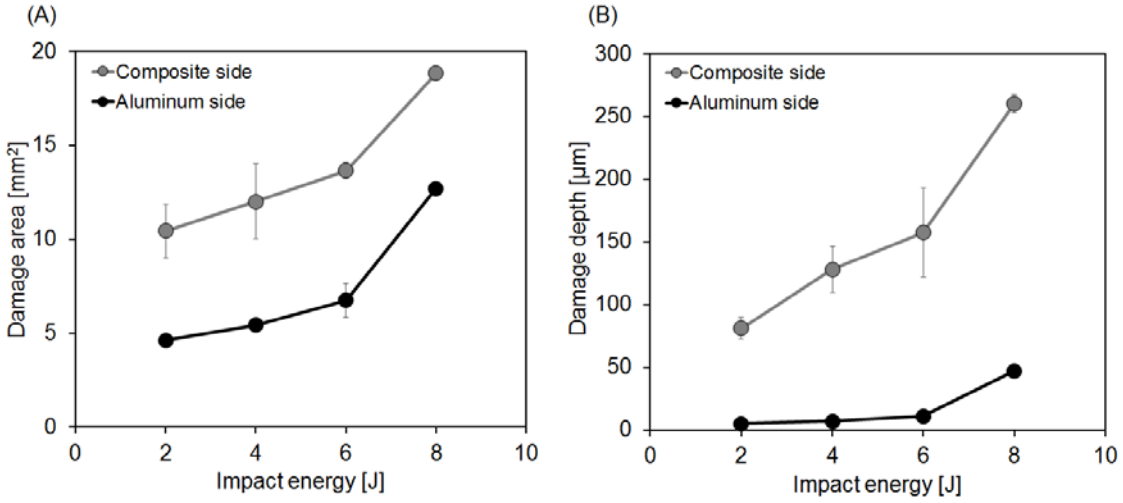

Figure 8: (A) Area of impact damage and (B) depth of impact damage for joints impacted from the aluminum and the composite sides for different levels of energy.

3.2.1. Damage development for aluminum-side impact

Figure 9 shows the damage caused by aluminum-side impact for 2 J, 4 J, 6 J and 8 J. The indentations left on the aluminum surfaces can be hardly identified in Figure 9. Therefore, dashed lines were used to highlight the impression on the aluminum surfaces after impact. In accordance with aircraft regulations, barely visible indentation damage (BVID) should not be identifiable at a distance of 50 cm during inspection [25]. Accordingly, the damages in this study were classified as BVID for all the investigated energy levels.

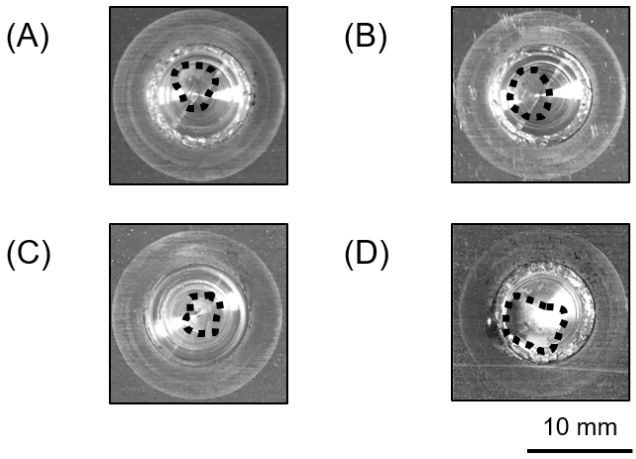

Figure 9: Damage evolution on the aluminum surface after (A) 2 J, (B) 4 J, (C) 6 J and (D) 8 J of impact energy. The dashed lines highlight the damage imprint on the aluminum surface.

On one hand, it was observed that the indenter locally generated very shallow impressions on the aluminum surfaces after impact (Figure 9). The damage deepened from 5.1 ± 0.3 µm to 47.3 ± 0.2 µm as the impact energy increased from 2 J to 8 J; the depths were evaluated using an adapted roughness measurement performed by laser confocal microscopy (Figure 8-B). On the other hand, a global bending of the aluminum part is noted (Figure 10). One observes that the angle of bending increased with the rise in impact energy. At 2 J, the bending angle was nearly 0° and aluminum and composite presented full contact in the overlap area of the joint. At 8 J, the bending angle reached approximately 10°. In this case, it was even observed that there was partial perforation of the composite part by the plastically deformed aluminum (arrow in Figure 10-D), leading to the detachment of the interface and failure of the joint during impact.

After impact, the joints were scanned with an ultrasound source to non-destructively evaluate the damage in the joints. No internal flaws could be observed in the aluminum part after impact. Nevertheless, the background echo from the ultrasound evaluation provided a qualitative comparison of the joint interface before and after impact. Since the output was very similar for all the investigated levels of impact energy, only a representative example is shown in Figure 11. The joint impacted with 4 J was selected for this purpose.

Figure 11 shows c-scans of the overlap area of a joint before and after impact on the aluminum surface. Before the impact event, it is possible to identify the unbonded areas of the overlap area along with the circular joined area, including the metallic nub in its center (Figure 11-B). After the impact event, the

echo signal inside the joined area became equal to the echo signal of the unbonded area (dark grey areas indicated by white arrows in Figure 11-C). It indicates that the contact between aluminum and composite was no longer present, suggesting the occurrence of detachment in the outer joined area. Additionally, a decrease in the intensity of the echo in the nub region was noted, indicating the occurrence of damage in that area as well.

These observations suggest that in the case of aluminum-side impact, the impact energy was absorbed by the joint as plastic deformation of the aluminum part, mostly. The bending of the aluminum introduced peeling stresses at the interface, which progressively promote the detachment of the interface and failure of the joint. Similar behavior was identified for bonded joints. Harris and Adams [32] investigated three types of aluminum alloys (soft, mild and hard) substrates to produce impact resistant adhesive bonded joints. Silva *et al.* [12] investigated steels (mild and high strength) and their impact behavior as substrates for adhesive bonded joints. In both studies, the global deformation of the metallic substrates due to impact were responsible to introduce stresses at the adhesive layer, decreasing the impact failure load of the joints. As a result, higher residual strengths were reported for the bonded joints produced with the stiffest substrates in [32] and [12].

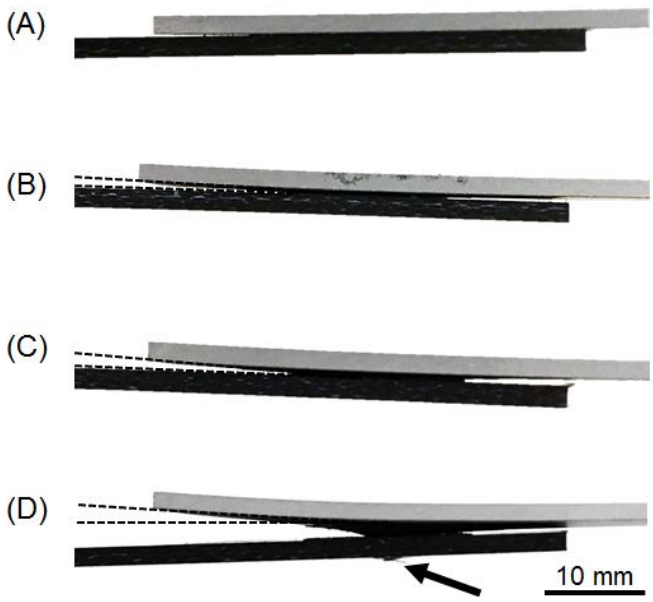

Figure 10: Representative side view of the joints after the impact on the aluminum surface for (A) 2 J, (B) 4 J, (C) 6 J and (D) 8 J (failed during impact).

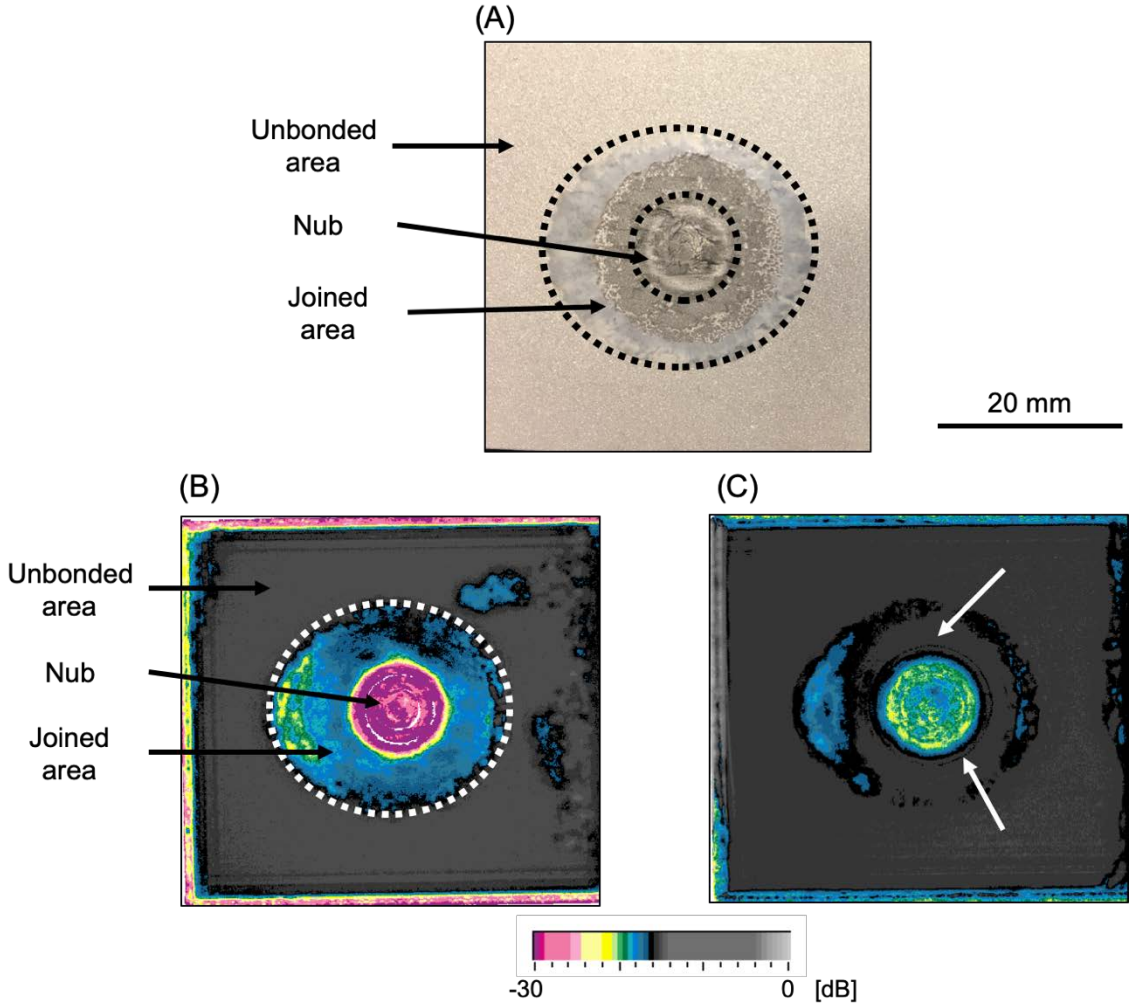

Figure 11: (A) Typical fracture surface of the aluminum part of a friction spot joint. Representative c-scans of the overlap area of a friction spot joint (B) before and (C) after impact on the aluminum surface. A joint impacted with 4 J was selected as a representative example in this qualitative analysis.

3.2.2. Damage development for composite-side impact

Figure 12 shows the damage caused by composite-side impact for 2 J, 4 J, 6 J and 8 J. As it was observed for the joints impacted from the aluminum side, the damages in this case were also classified as BVID for all the investigated energy levels [25].

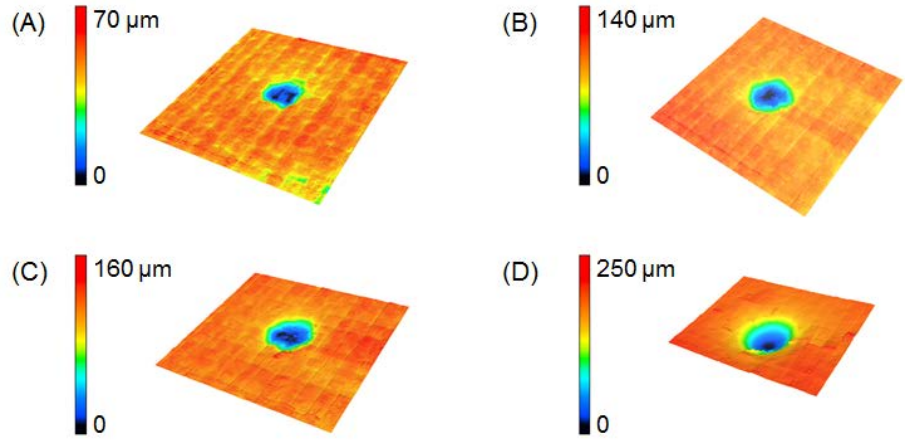

Figure 12: 3D images of the damage on the composite surface of the joints after (A) 2 J, (B) 4 J, (C) 6 J and (D) 8 J of impact energy.

One observes that the indenter locally penetrated the composite part during impact, contrary to the imprint observations on the aluminum-side impacted joints. It is possible to identify a depression on the composite surface after impact (Figure 12). Naturally, the CF-PPS presents lower hardness than the aluminum in this study (AA2024-T3: 1.4 GPa; CF-PPS: 0.4 GPa [33]), facilitating the penetration of the indenter.

Additionally, no global distortion was observed for the composite part after impact. Figure 13 shows that the composite and aluminum were still entirely in contact after impact, except for 8 J of impact energy. At 8 J, a distortion was observed on the aluminum part due to the high impact energy applied to the composite part (Figure 13-D). This distortion of the aluminum resulted in the detachment of the interface and failure of the joint during impact. The absence of distortion in the composite, even at high levels of impact energy, is considered a result of its layered structure [27]. It favors the energy absorption through the creation of internal and localized damage rather than a global path of energy dissipation [12,32].

Figure 14 shows the c-scans of the composite part before and after the impact event. The c-scans provided a qualitative comparison of the internal flaws in the composite part before and after impact. Since the output was very similar for all the investigated levels of impact energy, only a representative example is shown in Figure 14. The joint impacted with 4 J was selected for this purpose.

Before impact (Figure 14-B), it is possible to identify the presence of process-related defects through the thickness of the composite. One observes that such flaws are distributed in the center of the joint, inside a perimeter that corresponds to the area stirred by the sleeve during the joining process. In the

center of the joint, the highest temperatures are achieved during the joining process due to the proximity with the rotating tool [16]. As a result, more profound defects (middle thickness of the composite part, approximately 1 mm deep) were identified in the center of the joint, while superficial defects (close to the metal interface, approximately 2 mm deep) are found on its periphery. These process-related defects are basically microvoids originated from air entrapment during the outflow of molten/softened PPS matrix during the FSpJ process. The details on the formation of such flaws are found in [16,18,34]. After the impact event (Figure 14-C), one observes that the density of microvoids increased, especially in the center of the joint (at depths around 1 mm, green-colored defects). It indicates the occurrence of delamination and/or coalescence of previously damaged volumes due to the impact in that region.

These observations suggest that the impact energy was absorbed in the creation/extension of internal damage through the plies of the composite in the case of composite-side impact. Therefore, the impact energy was only partially transferred to the interface of the joint. This mechanism of energy absorption has been extensively reported in the literature for composite materials and adhesive bonded joints [27–29,35,36].

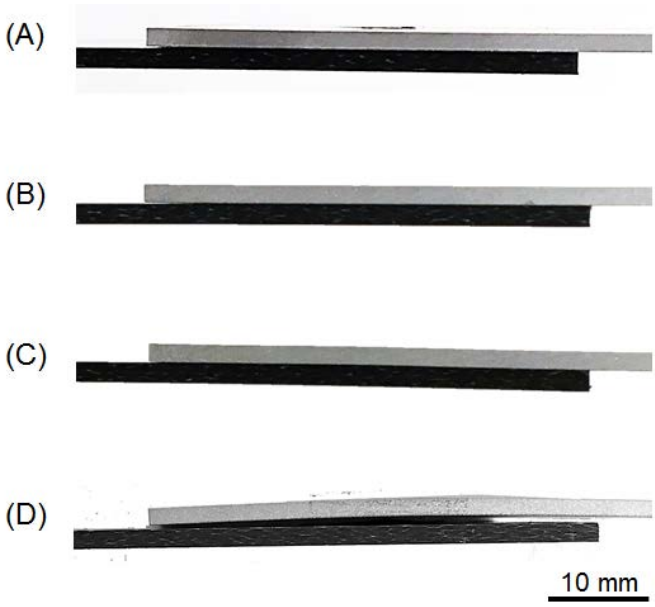

Figure 13: Representative side view of the joints after the impact on the composite surface for (A) 2 J, (B) 4 J, (C) 6 J and (D) 8 J (failed during impact).

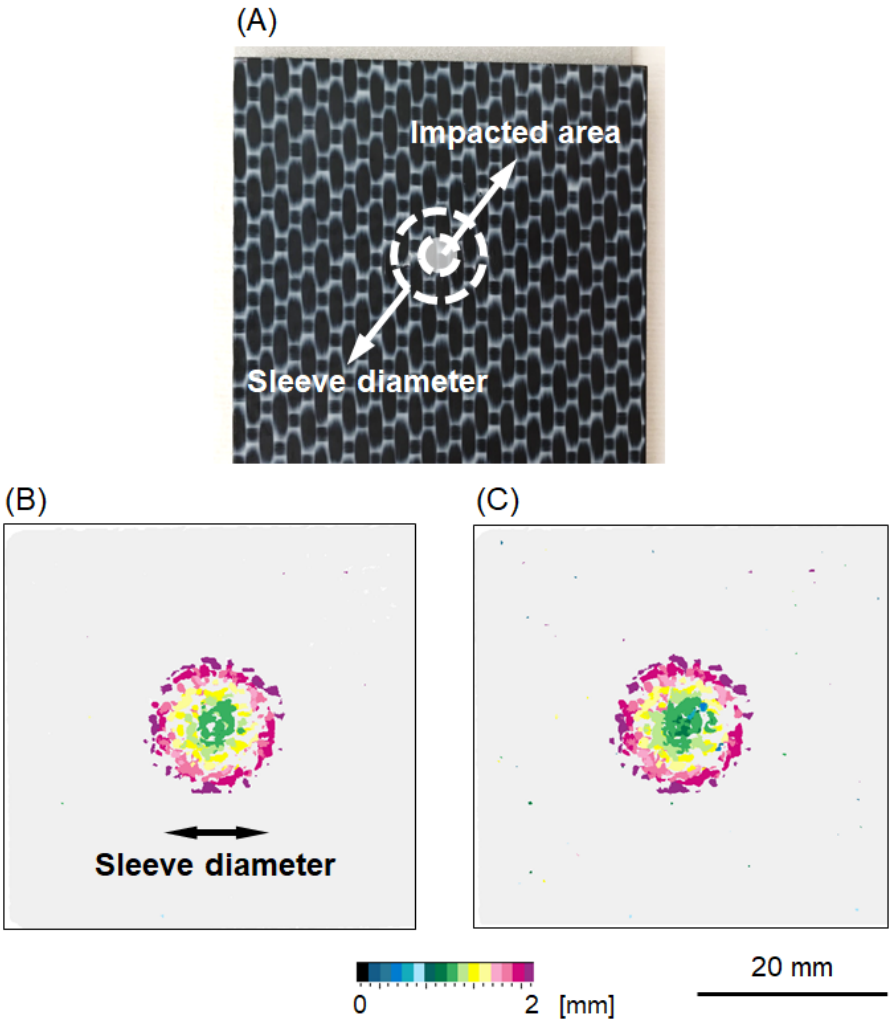

Figure 14: (A) Typical impacted composite surface showing the impacted area and the sleeve diameter used to perform the joining process. Representative c-scans through the thickness of the composite part on the overlap area of a friction spot joint (B) before and (C) after impact on the composite surface (4 J). (0 mm: composite surface under impact, and 2 mm: composite surface in contact with aluminum).

3.3. Residual shear strength after impact

Figure 15 presents the shear strength after impact (ShAI) of the joints for the different impact levels under investigation. One observes that the SSAI of the joints decreased progressively as the impact energy increased (Figure 15). The joints impacted from the aluminum side presented residual strengths of 84% (1735 ± 151 N) for 2 J, 30 % (624 ± 82 N) for 4 J, and 25% (523 ± 29 N) for 6 J impacts. For composite-side impacted joints, the residual strengths were 80% (1657 ± 86 N) for 2 J, 54% (1124 ± 45 N) for 4 J, and 45% (936 ± 242 N) for 6 J impact. The joints impacted with 8 J, for both AS and CS cases, failed during the impact event.

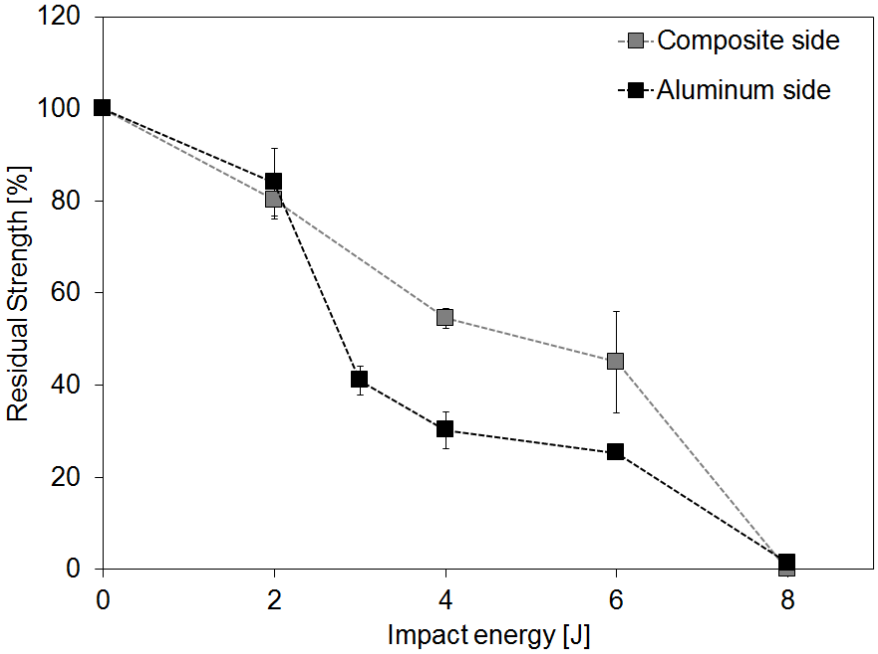

Figure 15: Shear strength after impact (SSAI) of the joints after impact.

Generally, the joints impacted from the aluminum side presented lower residual strength after impact than the joints impacted from the composite side (Figure 15). As previously discussed, the impact energy introduced from the aluminum side is mostly absorbed in the plastic deformation of the aluminum part. The bending of the aluminum promotes the detachment between aluminum and composite, advancing the damage at the interface as the bending angle increases (Figure 10). Otherwise, the impact energy introduced from the composite side is absorbed in the creation/extension of internal damage through the plies of the composite (Figure 14). Thus, it is expected that the impact energy was only partially transferred to the interface of the joint in the case of composite-side impact. Consequently, these joints showed higher residual strength after impact. Similar behavior was observed by Machado *et al.* [13]. The authors demonstrated that CFRP bonded joints presented higher impact failure loads than steel joints. They reported that the internal damages created in the CFRP substrates reduces the stresses in the adhesive layer of these joints in comparison to the steel joints, preserving its integrity.

Nevertheless, one also observes that for 2 J of impact energy the aluminum-side and composite-side impacted joints had similar residual strengths; 80 ± 4% for the composite-side and 84 ± 7% for the aluminum-side impact. As shown in Figure 10, the impact energy of 2 J was not sufficient to significantly bend the aluminum part of the joint. Therefore, it is expected that no additional peeling stresses were

introduced into the interface when the aluminum side of the joints was impacted in comparison to the composite-side impact case. As a result, the residual strength of the joints in this case are comparable.

These observations indicate that for low impact energy (2 J, in this study) the side of the joint under impact does not strongly affect the residual strength of the joint. Nevertheless, as the impact energy increases, the different impact behaviors of aluminum and composite play a more significant role in the strength degradation of the joint. The authors are aware that such observations are strongly influenced by the geometry of the coupons. Therefore, although this study for the first time assessed the damage behavior of the friction spot joints under impact, the upscaling of such results requires further investigations.

Figure 16 shows a typical fracture surface of the joints after impact and lap shear test. The main bonding zones of friction spot joints can be identified in the fracture surface: adhesion zone (AZ), transition zone (TZ) and plastically deformed zone (PDZ), including the nub deformation inside PDZ [16]. Nevertheless, no nuances were found on the fracture surface due to the impact event. The usual mixture of adhesive–cohesive failure mode was identified for the post-impact tested specimens. For a full analysis of this failure behavior of friction joints under tensile shear please refer to [16].

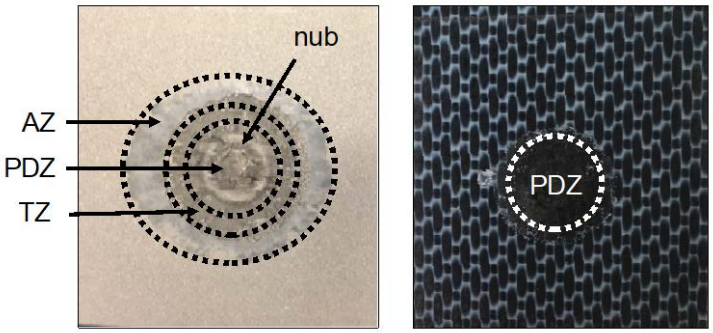

Figure 16: Fracture surface showing the main bonding zones of friction spot joints: adhesion zone (AZ), transition zone (TZ) and plastically deformed zone (PDZ), including the nub deformation inside PDZ.

4. Conclusions

The impact resistance of AA2024-T3/CF-PPS hybrid joints was investigated. The joints were aluminum-side and composite-side impacted. Four energy levels were investigated: 2 J, 4 J, 6 J and 8 J. It was observed that for each energy level the load applied by the impactor on the joint was very similar, independently of the surface under impact. The joints showed rebounding behavior for all the energy levels under investigation. It implies that, for all the cases, the impact energy was not entirely absorbed by the

joints, although the joints failed at 8 J of impact energy. It suggests that aluminum and composite could further absorb energy during an impact event. Nevertheless, the interface of the joint has its threshold for absorption of impact energy at around 6.5 J, which was reached when the joint was impacted with 8 J of potential energy (independently of the surface under impact). Thus, this study showed that a single friction spot joint could absorb up to 103 $kJ.m^{-2}$ of joined area, circa 50% higher than adhesive joints. Generally, the aluminum-side impacted joints presented lower residual strength after impact than the composite-side impacted joints. The impact energy introduced from the aluminum side was mostly absorbed in the plastic deformation of the aluminum part, bending the aluminum and promoting the detachment of the interface. On the other hand, the impact energy introduced from the composite side was mostly absorbed in the creation/extension of internal damage through the plies of the composite. Thus, it is expected that the impact energy is only partially transferred to the interface of the joint in the case of composite-side impact. Consequently, these joints presented higher residual strength after impact. Therefore, the impact resistance of these hybrid structures can be maximized when the composite part is the one majorly exposed to the impacts threats.

Acknowledgments

This work was supported by Helmholtz Association (Germany) and National Council for Scientific and Technological Development (Brazil, Process 200694/2015-4). S.T. Amancio-Filho would like to acknowledge “the Austrian aviation programme TAKE OFF” and “BMVIT-Austrian Ministry for Transport, Innovation and Technology” for their financial support.

References

[1] Flight Airworthiness Technology. Airbus Technical Magazine 2011; FAST 48.

[2] Rosenfeld M, editor. Damage Tolerance in Aircraft Structures. 100 Barr Harbor Drive, PO Box C700, West Conshohocken, PA 19428-2959: ASTM International; 1971.

[3] Engle R. Damage Accumulation Techniques in Damage Tolerance Analysis. In: Chang J, Rudd J, editors. Damage Tolerance of Metallic Structures: Analysis Methods and Applications, 100 Barr Harbor Drive, PO Box C700, West Conshohocken, PA 19428-2959: ASTM International; 1984, p. 25-25–11.

[4] Mallick PK. Materials, design and manufacturing for lightweight vehicles. 1st ed. Cambridge, UK: Woodhead Publishing Limited; 2010.

[5] Gudmundsson S. General Aviation Aircraft Design: Applied Methods and Procedures. 1st edition. S.l.: Butterworth-Heinemann; 2013.

[6] Potter D. Durability and Damage Tolerance Behavior of Adhesively Bonded Primary Structure. In: Abelkis P, Hudson C, editors. Design of Fatigue and Fracture Resistant Structures, 100 Barr Harbor Drive, PO Box C700, West Conshohocken, PA 19428-2959: ASTM International; 1982, p. 335-373.

[7] Alderliesten RC, Homan JJ. Fatigue and damage tolerance issues of Glare in aircraft structures. International Journal of Fatigue 2006;28:1116–23. doi:10.1016/j.ijfatigue.2006.02.015.

[8] Sadighi M, Alderliesten RC, Benedictus R. Impact resistance of fiber-metal laminates: A review. International Journal of Impact Engineering 2012;49:77–90. doi:10.1016/j.ijimpeng.2012.05.006.

[9] Qing X, Sun H-T, Dagba L, Chang F-K. Damage-Tolerance-Based Design of Bolted Composite Joints. In: Grant P, Rousseau C, editors. Composite Structures: Theory and Practice, 100 Barr Harbor Drive, PO Box C700, West Conshohocken, PA 19428-2959: ASTM International; 2001, p. 243-243–30.

[10] Johnson W, Masters J, Wilson D, Graesser D, Tuttle M. Damage Tolerance Predictions for Stiffened Composite Panels—Part II: Application of a Failure Criteria. Journal of Composites Technology and Research 1996;18:102. doi:10.1520/CTR10521J.

[11] Liu Y, Liaw B. Effects of Constituents and Lay-up Configuration on Drop-Weight Tests of Fiber-Metal Laminates. Appl Compos Mater 2010;17:43–62. doi:10.1007/s10443-009-9119-1.

[12] Silva MRG, Marques E a. S, Silva LFM da, Silva MRG, Marques E a. S, Silva LFM da. Behaviour under Impact of Mixed Adhesive Joints for the Automotive Industry. Latin American Journal of Solids and Structures 2016;13:835–53. doi:10.1590/1679-78252762.

[13] Machado JJM, Gamarra PM-R, Marques EAS, da Silva LFM. Improvement in impact strength of composite joints for the automotive industry. Composites Part B: Engineering 2018;138:243–55. doi:10.1016/j.compositesb.2017.11.038.

[14] Amancio-Filho ST, dos Santos J. European Patent 2329905B1, 2012.

[15] Amancio-Filho ST, Bueno C, dos Santos JF, Huber N, Hage Jr. E. On the feasibility of friction spot joining in magnesium/fiber-reinforced polymer composite hybrid structures. Materials Science and Engineering: A 2011;528:3841–8. doi:10.1016/j.msea.2011.01.085.

[16] Goushegir SM, dos Santos JF, Amancio-Filho ST. Friction Spot Joining of Aluminum AA2024 / Carbon-Fiber Reinforced Poly(phenylene sulfide)composite single lap joints: microstructure and mechanical performance. Materials & Design 2014;50:196–206. doi:10.1016/j.matdes.2013.08.034.

[17] Goushegir SM. Friction spot joining (FSpJ) of aluminum-CFRP hybrid structures. Weld World 2016;60:1073–93. doi:10.1007/s40194-016-0368-y.

[18] André NM, Goushegir SM, dos Santos JF, Canto LB, Amancio-Filho ST. Friction Spot Joining of aluminum alloy 2024-T3 and carbon-fiber-reinforced poly(phenylene sulfide) laminate with additional PPS film interlayer: Microstructure, mechanical strength and failure mechanisms. Composites Part B: Engineering 2016;94:197–208. doi:10.1016/j.compositesb.2016.03.011.

[19] Esteves JV, Goushegir SM, dos Santos JF, Canto LB, Hage Jr. E, Amancio-Filho ST. Friction spot joining of aluminum AA6181-T4 and carbon fiber-reinforced poly(phenylene sulfide): Effects of process parameters on the microstructure and mechanical strength. Materials & Design 2015;66:437–45. doi:10.1016/j.matdes.2014.06.070.

[20] American Society for Metals, American Society for Metals. Metals Handbook. Volume 2. Metals Park, Ohio: American Society for Metals; 1981.

[21] Aluminum alloy 2024-T3 technical datasheet. Constellium, France, 2012.

[22] CETEX® PPS technical datasheet. Tencate Advanced Composites, Netherlands, 2009.

[23] Airframers - TenCate Advanced Composites (Netherlands). <http://www.airframer.com/direct_detail.html?company=131248>. Accessed: October 2018.

[24] André NM, Goushegir SM, Scharnagl N, Santos JF dos, Canto LB, Amancio-Filho ST. Composite surface pre-treatments: Improvement on adhesion mechanisms and mechanical performance of metal–composite friction spot joints with additional film interlayer. The Journal of Adhesion 2017;0:1–20. doi:10.1080/00218464.2017.1378101.

[25] Airbus. Composites Airbus: Damage Tolerance Methodology, Chicago, USA: 2006.<https://www.niar.wichita.edu/chicagoworkshop/Chicago%20Damage%20Tlerance%20Workshop%20%20July%201921,%202006/Wednesday%20%20Session%201%20Presentations/Airbus%20Composites%20%20Damage%20Tolerance%20Methodolgy%20-%20Fualdes.pdf>. Access: June 2018.

[26] Bieniaś J, Jakubczak P, Surowska B, Dragan K. Low-energy impact behaviour and damage characterization of carbon fibre reinforced polymer and aluminium hybrid laminates. Archives of Civil and Mechanical Engineering 2015;15:925–32. doi:10.1016/j.acme.2014.09.007.

[27] Liu D. Impact-Induced Delamination—A View of Bending Stiffness Mismatching. Journal of Composite Materials 1988;22:674–92. doi:10.1177/002199838802200706.

[28] Aktaş M, Atas C, İçten BM, Karakuzu R. An experimental investigation of the impact response of composite laminates. Composite Structures 2009;87:307–13. doi:10.1016/j.compstruct.2008.02.003.

[29] Machado JJM, Marques E a. S, da Silva LFM. Adhesives and adhesive joints under impact loadings: An overview. J Adhes 2018;94:421–52. doi:10.1080/00218464.2017.1282349.

[30] Boria S, Scattina A, Belingardi G. Impact behavior of a fully thermoplastic composite. Composite Structures 2017;167:63–75. doi:10.1016/j.compstruct.2017.01.083.

[31] Roesler J, Harders H, Baeker M. Mechanical Behavior of Engineering Materials: Metals, Ceramics, Polymers, and Composites. 1st ed. Germany: Springer; 2007.

[32] Harris JA, Adams RD. An Assessment of the Impact Performance of Bonded Joints for Use in High Energy Absorbing Structures , An Assessment of the Impact Performance of Bonded Joints for Use in High Energy Absorbing Structures. Proceedings of the Institution of Mechanical Engineers, Part C: Journal of Mechanical Engineering Science 1985;199:121–31. doi:10.1243/PIME_PROC_1985_199_102_02.

[33] André NM. Friction Spot Joining of aluminum alloy 2024-T3 and carbon-fiber-reinforced polyphenylene sulfide composite laminate with additional PPS film interlayer. Master thesis. Federal University of São Carlos, 2015.

[34] André NM, Goushegir SM, Dos Santos JF, Canto LB, Amancio-Filho S de T. Influência termomecânica do processo de União Pontual por Fricção na recristalizaçãodos componentes poliméricos de junta híbrida CF-PPS/Alumínio com filme intermediário de PPS. In: Brazilian National Congress of Polymers, Natal - RN, Brasil: 2015.

[35] Ozdemir O, Oztoprak N. An investigation into the effects of fabric reinforcements in the bonding surface on failure response and transverse impact behavior of adhesively bonded dissimilar joints. Composites Part B: Engineering 2017;126:72–80. doi:10.1016/j.compositesb.2017.06.005.

508 [36] Choudhry RS, Hassan SF, Li S, Day R. Damage in single lap joints of woven fabric reinforced
509 polymeric composites subjected to transverse impact loading. International Journal of Impact Engineering
510 2015;80:76–93. doi:10.1016/j.ijimpeng.2015.02.003.
511